https://doi.org/10.5194/egusphere-2025-957
Preprint. Discussion started: 12 March 2025


# Sedimentary organic carbon dynamics in a glaciated Arctic fjord: tracing contributions of terrestrial and marine sources in the context of Atlantification over recent centuries

Dahae Kim[a], Jung-Hyun Kim[a,*], Youngkyu Ahn[a], Matthias Forwick[b], Seung-Il Nam[a]

[a]Korea Polar Research Institute, 26 Songdomirae-ro, Yeonsu-gu, Incheon 21990, South Korea

[b]UiT The Arctic University of Norway, Department of Geosciences, NO-9037 Tromsø, Norway

***Correspondence:**

Jung-Hyun Kim (jhkim123@kopri.re.kr)

https://doi.org/10.5194/egusphere-2025-957
Preprint. Discussion started: 12 March 2025


**Abstract**

In this study, we investigated sedimentary organic carbon (OC) dynamics in Kongsfjorden, Svalbard, using three multicores collected during the HH22 and HH23 cruises aboard the RV *Helmer Hanssen* in 2022 and 2023. We assessed the relative contributions of petrogenic, soil-derived, plant-derived, and marine OC by applying a four-source apportionment approach based on $\Delta^{14}C_{org}$, $\delta^{13}C_{org}$, and lignin parameters, including the $(Ad/Al)_v$ ratio and lignin phenol concentrations, with Monte Carlo (MC) analysis. Age-depth models based on $^{210}Pb$ and $^{226}Ra$ data were used to evaluate temporal variations in the accumulation rates (ARs) of sedimentary OC. Our findings revealed a significant increase in marine OC ARs in recent decades, which appears to be closely linked to enhanced Atlantic Water (AW) inflow. This trend suggests that changes in the fjord's biogeochemical cycles, driven by AW, are influencing sedimentary OC dynamics. Consequently, the increasing influence of AW underscores the potential for ongoing Arctic warming to further amplify AW inflow into Arctic fjords, with significant implications for carbon cycling and fjord ecosystems. By providing a historical perspective on AW trends and their effects on sedimentary OC dynamics, this study offers valuable insights into the potential consequences of future climate change.

Keywords: Svalbard, Kongsfjorden, organic carbon, stable isotopes, radiocarbon isotopes, lignin phenols

https://doi.org/10.5194/egusphere-2025-957
Preprint. Discussion started: 12 March 2025


## Introduction

The Arctic region is currently experiencing rapid climate change, with surface air temperatures rising nearly four times faster than the global average since 1979 (Rantanen et al., 2022). This accelerated warming has profound implications for the region's ecosystems and carbon dynamics (Dahlke et al., 2020; Friedlingstein et al., 2020). In particular, Arctic fjords are known for their high sediment accumulation rates, receiving substantial terrestrial input from glacial meltwater and erosional processes (Winkelmann and Knies, 2005). As a result, these fjords serve as critical hotspots for global organic carbon (OC) burial and provide valuable archives for high-resolution environmental records (Smith et al., 2015; Bianchi et al., 2020). Due to the extreme warming rates observed, Arctic fjords are increasingly vulnerable to climate change impacts, which reflect broader shifts occurring across the Arctic system. While modern observations have clear limitations in providing long-term datasets, past episodes of climate change preserved in sediment cores and other environmental archives offer a unique opportunity to reconstruct and understand the response of OC dynamics since the 20th century (Ingrosso et al., 2025).

The high-Arctic Svalbard archipelago, a key region at the interface of the North Atlantic and Arctic Oceans, is characterized by glaciers occupying approximately 57% of its landmasses (Nuth et al., 2013). A significant driver of environmental change in Svalbard is the enhanced inflow of warm and saline Atlantic Water (AW) transported by the West Spitsbergen Current (WSC), which influences the western coast of Spitsbergen, the largest island in the archipelago (De Rovere et al., 2022). This process, termed Atlantification, has intensified in recent decades, accelerating the decline of summer sea ice extent, enhancing tidewater glacier melting, and increasing freshwater discharge into fjords (e.g., Jernas et al., 2018; Krajewska et al., 2020; Skogseth et al., 2020). Kongsfjorden, located on the western coast of Spitsbergen, has emerged as a critical site for studying the effects of recent Arctic warming due to its dynamic and highly sensitive environment (e.g., Tesi et al., 2021).

Despite substantial research on spatial sedimentary OC variability in Kongsfjorden using bulk elemental and isotopic parameters, molecular-level studies on sedimentary OC sources remain limited, particularly over recent decades. Furthermore, the long-term changes driven by ongoing Atlantification since the mid-1990s have yet to be explored (e.g., Årthun et al., 2012; Polyakov et al., 2017; Lind et al., 2018; Tesi et al., 2021). The lack of long-term observational and historical data on AW inflow in this region highlights

https://doi.org/10.5194/egusphere-2025-957
Preprint. Discussion started: 12 March 2025


the urgent need for sedimentary records to establish baselines and quantify rates of environmental change (e.g., Tesi et al., 2021; Jordà-Molina et al., 2023; Cottier et al., 2007). Such records are invaluable for distinguishing between natural variability and human-induced changes, providing insights into the mechanisms driving environmental changes in Arctic fjords.

In this study, we address these gaps by analyzing three multicores collected from Kongsfjorden to: (1) characterize sedimentary OC along a transect from the inner to the outer fjord, (2) estimate temporal variations in the relative contributions of sedimentary OC sources over the past centuries, and (3) assess the impact of human-induced climate variability on environmental changes. Using a combination of bulk geochemical parameters (carbon and nitrogen contents, stable carbon and radiocarbon isotopes), molecular analyses (lignin phenols), and sedimentological measurements (bulk dry density, grain size, and surface area), our study provides critical insights into the interplay between terrestrial and marine systems, and highlights their sensitivity to ongoing and future climate change.

## 2. Material and methods

### 2.1 Regional setting

Kongsfjorden, located on the western coast of Spitsbergen, Svalbard, is a fjord system with a drainage basin of approximately 1440 km², 80% of which is covered by glaciers (Pramanik et al., 2020). The fjord is about 27 km long, 4 to 10 km wide, and has a volume of approximately 29.4 km³ (Ito & Kudoh, 1997; Brogi et al., 2019). The system is shaped by inputs from five major glaciers—Kongsvegen, Kronebreen, Kongsbreen, Conwaybreen, and Blomstrandbreen—and the Bayelva River (Zhu et al., 2016; McGovern et al., 2022). Kongsfjorden is influenced by the intrusion of relatively warm (~6°C), nutrient-rich Atlantic Water due to the absence of a sill at the fjord's mouth, which impacts both hydrology and biogeochemistry (Svendsen et al., 2002; Tverberg et al., 2019). The fjord is part of the Kongsfjorden-Krossfjorden system, where both fjords merge into the Kongsfjordrenna trough, which cross-cuts the continental shelf offshore of northwestern Spitsbergen (Svendsen et al., 2002). The system experiences an exchange of Atlantic and Arctic Waters, and glacial meltwaters at the West Spitsbergen Shelf, contributing to long-range marine transport processes (Choudhary et al., 2022; Saloranta and Svendsen, 2001). Glacial runoff delivers large volumes of sediment to the seabed, forming turbid plumes that restrict the euphotic zone and primary productivity,

https://doi.org/10.5194/egusphere-2025-957
Preprint. Discussion started: 12 March 2025


particularly near the glaciers (Ito and Kudoh, 1997; Svendsen et al., 2002). Despite limited primary productivity in some areas, the fjord's relatively long water residence time and slower exchange rate, compared to the open ocean, result in significant local circulation and water mass distribution within the system (Herzke et al., 2021).

### 2.2 Sample collection

Three multicores were recovered from Kongsfjorden, Svalbard, at water depths of 81 m (core HH23-1058MUC, hereafter 1058MUC; 45 cm long), 339 m (core HH22-1161MUC, hereafter 1161MUC; 44 cm long), and 323 m (core HH22-1159MUC, hereafter 1159MUC; 40 cm long) during the RV *Helmer Hanssen* cruises (HH22 and HH23) in 2022 and 2023 (Fig. 1 and Table S1). The cores were retrieved using a multi-corer (KC Denmark model 72.000, with 6 core liners; 11 cm outer diameter; 10.5 cm inner diameter, and 0.8 m length each). The multicores were sectioned into 1 cm intervals onboard and stored at –20°C. Subsequently, the samples were freeze-dried for further analysis.

### 2.3 Sedimentological analysis

Water content was calculated by determining the weight loss of wet bulk samples after freeze-drying. The dry bulk density of homogenized subsamples was measured using an AccuPyc II 1345 pycnometer (Micromeritics, Georgia, USA) at KOPRI. The average of three measurements was used for grain density calculations to ensure precision, with an analytical error of less than 0.0032 $cm^3$ observed when employing the 1 $cm^3$ chamber.

Grain size distribution followed the methodology outlined by Ahn et al. (2024). Approximately 130 mg of freeze-dried, unground subsamples were treated with 5 mL of 35% $H_2O_2$ to oxidize organic matter. A Mastersizer 3000 laser particle size analyzer (Malvern Panalytical B.V., UK) was used for grain size analysis of bulk sediments at KOPRI. Analytical precision was determined as follows: D(10): 37.5 ± 0.3 μm, D(50): 71.4 ± 0.2 μm, D(90): 104.0 ± 0.0 μm.

Specific surface area (SA) measurements were conducted following the method described by Kim et al. (2022). Freeze-dried, unground subsamples were first heated to remove organic matter and then cooled gradually over 12 hours to room temperature. Prior to analysis, the samples were degassed at 200°C for 2 hours under a constant flow of $N_2$ gas using a Micromeritics FlowPrep 060 Sample Degas System at the Korea Basic

https://doi.org/10.5194/egusphere-2025-957
Preprint. Discussion started: 12 March 2025


Science Institute (KBSI, Jeonju Center). Specific SA was measured with $N_2$ gas as the adsorbate in a He atmosphere, with an analytical precision within ± 9%. Instrument performance was verified using Carbon Black (21.0 ± 0.75 $m^2/g$; ISO 9277:2010), a certified reference material provided by Micromeritics.

**2.4 Radioisotope analysis**

Freeze-dried and ground subsamples (~5 g) were subjected to gamma spectrometry analysis using a well-type HPGe detector at KBSI to measure the activities of $^{210}Pb$ and $^{226}Ra$. The analytical uncertainties averaged 9.6 ± 2.0 mBq/g for $^{210}Pb$ and 2.7 ± 4.1 mBq/g for $^{226}Ra$. Excess $^{210}Pb$ ($^{210}Pb_{ex}$) activities were calculated by subtracting the $^{226}Ra$ activity from the total $^{210}Pb$ ($^{210}Pb_{tot}$) activity, following the approach described by Appleby (1998). The apparent sedimentation rate (cm/yr) was calculated from $^{210}Pb_{ex}$ with the constant rate of supply (CRS) model (cf. Appleby and Oldfield, 1978) with the following equation:

$$\text{Apparent sedimentation rate} = -\lambda / b \text{ (cm/yr)} \quad (1)$$

where λ is the radioisotope decay constant for $^{210}Pb$ (0.03114 per year), and *b* is the slope of the regression line.

**2.5 Bulk elemental and carbon isotope analysis**

The bulk elemental and carbon isotopic composition were determined using the procedure based on Kim et al. (2023). In brief, total nitrogen ($N_{tot}$) and total organic carbon (TOC) contents, as well as carbon isotopic compositions ($\delta^{13}C_{org}$), were analyzed using an elemental analyzer (Thermo Electron Corporation Flash EA 2000, Thermo Fisher Scientific, Germany) connected to an isotope ratio mass spectrometer (Finnigan Delta Plus, Thermo Fisher Scientific, Germany). TOC and $\delta^{13}C_{org}$ were measured on decalcified samples using 1 M HCl for 24 hours. The $\delta^{13}C_{org}$ values were expressed in delta notation (‰) relative to the Vienna Pee Dee Belemnite (VPDB) standard. The analytical precision was within 0.5 wt. % for carbon, 0.5 wt. % for nitrogen, and 0.5‰ for carbon isotopes.

Radiocarbon ($^{14}C$) analysis of TOC was carried out using accelerator mass spectrometry (AMS) at the Center for Applied Isotope Studies at the University of

https://doi.org/10.5194/egusphere-2025-957
Preprint. Discussion started: 12 March 2025


Georgia (CAIS, Georgia, USA). The radiocarbon results were presented in delta notation ($\Delta^{14}C_{org}$, ‰), as defined by Stuiver and Polach (1977).

### 2.6 Lignin phenol analysis

The CuO oxidation of samples and subsequent analyses were performed following the procedure from Kim et al. (2023). In brief, homogenized subsamples (~400 mg) were subjected to alkaline CuO oxidation in the presence of cupric oxide and ammonium iron (II) sulfate hexahydrate. This process was conducted using a Microwave Digestion System (MARS 6 microwave, CEM Corporation, USA) at 150℃ for 1.5 hours after adding $N_2$-purged NaOH solution. After oxidation, a known amount of internal standard (ethyl vanillin) was added to the CuO oxidation products. The resulting products were analyzed at KOPRI using an Agilent 7890B gas chromatograph (GC) coupled to a 5977B Series Mass Selective Detector (MSD) (Agilent Technologies, Santa Clara, CA, USA). Analyses were conducted in single ion monitoring (SIM) mode with a DB1-MS capillary column (30 m × 0.25 mm, 0.25 μm, Agilent J&W). The analytical precision for lignin phenols concentrations, determined through replicate measurements of the same sediment samples, was typically less than 10%. Calibration was performed using commercially available standards.

## 3. Results

### 3.1 Sediment properties

The depth profiles of water content, dry bulk density, grain size distribution, mean grain size, and specific surface area (SA) for the three cores are shown in Fig. 2 and Table S2. Water content displayed distinct trends across the cores. The highest water content was observed at the outermost site (core 1159MUC), ranging from 30.3% to 47.5%, with an average of 38.5 ± 3.2%. At the middle site (core 1161MUC), water content ranged from 31.7% to 42.2%, with an average of 35.3 ± 2.2%. The innermost site (core 1058MUC) exhibited the lowest range, from 19.7% to 32.6%, with an average of 27.9 ± 2.3%.

Dry bulk density measurements showed a decreasing trend from the innermost to the outermost core. Core 1058MUC had a dry bulk density ranging from 2.74 g/cc to 2.77 g/cc, for core 1161MUC, the range was 2.68 g/cc to 2.80 g/cc. For core 1159MUC, the range was 2.60 g/cc to 2.69 g/cc.

https://doi.org/10.5194/egusphere-2025-957
Preprint. Discussion started: 12 March 2025


In general, silt content was predominant in all three cores, with the highest average observed at the innermost site (core 1058MUC), where it reached 90 ± 2%. Mean grain sizes varied across the sites, with the innermost site (core 1058MUC) showing the largest grain sizes, ranging from 8.8 µm to 13.3 µm. The middle site (core 1161MUC) exhibited a slightly smaller range, from 7.9 µm to 13.0 µm, while the outermost site (core 1159MUC) ranged from 8.3 µm to 11.0 µm.

Mineral-specific surface area (SA) values decreased with distance from the inner fjord site. Core 1058MUC showed values between 10.0 $m^2/g$ and 16.5 $m^2/g$, core 1161MUC ranged from 8.6 $m^2/g$ to 13.9 $m^2/g$, and core 1159MUC exhibited the lowest range, from 8.3 $m^2/g$ to 11.0 $m^2/g$.

### 3.2 $^{210}$Pb geochronology

The depth profiles of total $^{210}$Pb ($^{210}Pb_{tot}$) and excess $^{210}$Pb ($^{210}Pb_{ex}$) activities for the two cores are displayed in Fig. 3 and summarized in Table S3. Core 1161MUC exhibited $^{210}Pb_{tot}$ values ranging from 89.3 mBq/g to 233.0 mBq/g, while the core 1159MUC showed a broader range from 22.1 mBq/g to 246.6 mBq/g. For $^{210}Pb_{ex}$, core 1161MUC had values between 59.6 mBq/g and 207.2 mBq/g, the core 1159MUC displayed a range from 9.3 mBq/g to 216.0 mBq/g. Based on these data, the mean sedimentation rate (SR) was calculated as 0.36 cm/yr at the middle site (core 1161MUC) and 0.12 cm/yr at the outermost site (core 1159MUC), comparable to the 0.15 cm/yr reported for Kongsfjorden (Zaborska et al., 2006).

### 3.3 Bulk elemental and carbon isotopic compositions

The depth profiles of bulk elemental and carbon isotope parameters for the three sediment cores are shown in Fig. 4 and summarized in Table S3. The TOC content showed clear trends depending on the core location. Core 1058MUC had values ranging from 0.2 to 0.4 wt.% (mean 0.3 ± 0.0 wt.%), while core 1161MUC ranged from 0.9 to 1.5 wt.% (mean 1.2 ± 0.1 wt.%), and core 1159MUC exhibited the highest values, ranging from 1.9 to 2.5 wt.% (mean 2.2 ± 0.2 wt.%). A similar pattern was observed for total nitrogen ($N_{tot}$) content: core 1058MUC ranged from 0.01 to 0.05 wt.%, core 1161MUC ranged from 0.08 to 0.13 wt.%, and core 1159MUC exhibited values from 0.22 to 0.26 wt.%. Previous studies conducted in Svalbard fjords, particularly in Kongsfjorden, have shown that surface sediments contain a substantial contribution of inorganic nitrogen (up to 70% of the $N_{tot}$ content, Fig. S1), with a significant correlation between inorganic

https://doi.org/10.5194/egusphere-2025-957
Preprint. Discussion started: 12 March 2025


nitrogen (N) and clay minerals (Kim et al., 2023; Winkelmann & Knies, 2005; Knies & Martinez, 2009; Kumar et al., 2016; Knies et al., 2007; Schubert & Calvert, 2001). Therefore, the $N_{org}$ values for the three sediment cores were estimated using the correlation between $N_{tot}$ and $N_{org}$ in Kongsfjorden surface sediments established in previous studies (Fig. S1). The resulting organic nitrogen ($N_{org}$) contents ranged from 0.01 to 0.03 wt.% (mean 0.01 ± 0.00 wt.%) for core 1058MUC, from 0.05 to 0.09 wt.% (mean 0.07 ± 0.01 wt.%) for core 1161MUC, and from 0.14 to 0.17 wt.% (mean 0.15 ± 0.01 wt.%) for core 1159MUC.

The molar $N_{tot}$/TOC ratios were lowest in core 1058MUC, varying from 0.04 to 0.12 (average 0.06 ± 0.02), followed by core1161MUC, ranging from 0.06 to 0.11 (average 0.07 ± 0.01), and core 1159MUC with values between 0.08 and 0.11 (average 0.09 ± 0.01). The $N_{org}$/TOC ratios showed a similar pattern, being lower than the corresponding $N_{tot}$/TOC ratios, with core 1058MUC ranging from 0.03 to 0.08, core 1161MUC ranging from 0.04 to 0.07, and core1159MUC ranging from 0.05 to 0.07.

The $\delta^{13}C_{org}$ values exhibited an offshore-increasing trend: core 1058MUC had values between –24.6‰ and –22.5‰ (average –23.5 ± 0.5 ‰), core 1161MUC ranged from –23.9‰ to –22.3‰ (average –23.2 ± 0.3 ‰), and core 1159MUC showed the most enriched values, ranging from –23.5‰ to –22.4‰ (average –22.7 ± 0.3 ‰). Similarly, $\Delta^{14}C_{org}$ values increased from the innermost to the outermost site: core 1058MUC ranged from –839.2‰ to –743.5‰ (average –793.9 ± 31.1 ‰), core 1161MUC ranged from –555.9‰ to –405.7‰ (average –504.9 ± 44.0 ‰), and core 1159MUC ranged from –469.3‰ to –396.7‰ (average –433.5 ± 21.7 ‰).

### 3.4 Lignin phenol compositions

The depth profiles of the products of alkaline CuO oxidation for the three sediment cores are presented in Fig. 5 and summarized in Table S4. Total lignin phenol concentrations, which represent the sum of eight lignin-derived monomeric phenols (vanillyl (V), syringyl (S), and cinnamyl (C) units), normalized to TOC, showed clear variation with depth and location. Core 1058MUC had the highest total lignin phenol concentrations, ranging from 0.24 mg/gOC to 0.66 mg/gOC (mean 0.40 ± 0.12 mg/gOC). In contrast, core 1161MUC had lower values, ranging from 0.07 mg/gOC to 0.19 mg/gOC (mean 0.14 ± 0.04 mg/gOC), and core 1159MUC exhibited the lowest concentrations, ranging from 0.06 mg/gOC to 0.22 mg/gOC (mean 0.12 ± 0.04 mg/gOC).

https://doi.org/10.5194/egusphere-2025-957
Preprint. Discussion started: 12 March 2025


The S/V and C/V ratios, which are indicative of the source and type of organic material, followed a similar pattern, with higher values at the innermost site. For core 1058MUC, the S/V ratio ranged from 0.01 to 0.63, and the C/V ratio ranged from 0.00 to 0.55. At the middle site (core 1161MUC), the S/V ratio ranged from 0.07 to 0.36, and the C/V ratio ranged from 0.00 to 0.25, both showing a decrease towards the outer site. Core 1159MUC (outer) showed values from 0.13 to 0.49 for S/V and from 0.14 to 0.41 for C/V, which were higher than those at the middle site but still lower compared to the innermost core.

The 3,5-Bd/V ratios, which indicate the degradation status of lignin oxidation, varied significantly across the sites. For core 1058MUC, values ranged from 0.06 to 0.55, while core 1161MUC showed a wider range from 0.47 to 2.59. Core 1159MUC exhibited the highest 3,5-Bd/V ratios, ranging from 0.59 to 2.46, indicating more extensive oxidation processes at the outer site compared to the inner sites. The (Ad/Al)v ratios, which represent the degree of lignin alteration, followed a similar trend. Core 1058MUC had values ranging from 0.22 to 0.89, while core 1161MUC (middle) ranged from 0.40 to 1.60. The highest values were observed in core 1159MUC (outer), ranging from 0.37 to 1.74, further supporting the trend of increased alteration in sediments towards the outer fjord.

## 4. Discussion

### 4.1 Grain size end-member modelling

Grain-size end-member (EM) modeling identifies representative patterns within a sediment's grain-size distribution, allowing for inferences about the influence of depositional processes based on variations in the relative abundances of each EM (van Hateren et al., 2018). Following the approach used by Ahn et al. (2024) in Wijdefjorden, northern Svalbard, grain-size EM modeling was performed to analyze variations in the grain-size distribution of the three cores investigated in this study. Two candidate Q values were identified (Fig. S2), with $R^2$ values exceeding 0.6 for each core (Fig. S3). The optimal Q value was selected by comparing the extracted EMs with the analyzed grain-size distribution curves (Fig. S4). From the three cores, a total of eight EMs were extracted (Fig. S5) and subsequently classified into four primary EM groups (Fig. 6A). EM1 primarily consisted of fine-grained sediment (very fine to medium silt, 2–16 μm), with EM1b having a relatively coarser-dominant mode (primary mode: 9.3–15.5 μm, very

https://doi.org/10.5194/egusphere-2025-957
Preprint. Discussion started: 12 March 2025


fine to medium silt: 54.3–59.7%) compared to EM1a (primary mode: 8.2–9.3 μm, very fine to medium silt: 62.2–66.8%). In contrast, EM2 was dominated by coarser grains (medium to very coarse silt, 8–63 μm, 66.4%), with a coarse primary mode of 29.3 μm. Notably, EM3 exhibited a wide range of grain sizes, including both fine and coarse particles, with modes at 9.3 and 81.2 μm.

The EM results revealed that EM1a and EM1b, primarily consisting of the finest grains, were present in all three sediment cores (Fig. 6B). These fine-grained sediments are generally deposited through size-dependent settling of suspended particles from meltwater and/or glaciofluvial discharge (Ó Cofaigh and Dowdeswell, 2001; Forwick and Vorren, 2009; Elverhøi et al., 1980). The flocculation in seawater further promotes their settling (Meslard et al., 2018), facilitating the transport of both EM1a and EM1b from the inner to the outer fjord. The distinction between EM1a and EM1b deposition is influenced by the strength of meltwater discharge, with stronger discharge suspending and transporting relatively coarser particles found in EM1b (Ahn et al., 2024). In contrast, coarse-grained sediments, primarily represented by EM2, were observed only in the innermost core 1058MUC, located closest to the glacier front (Fig. 6B). This area, near the glacier front, is likely influenced by outflowing bottom currents driven by subglacial meltwater (Meslard et al., 2018; Torsvik et al., 2019). The scarcity of fine particles in EM2 can be attributed to the winnowing effect of these currents, which preferentially remove finer material, leaving behind coarser particles (Vorren et al., 1984). Additionally, glacial sediments are typically poorly sorted, which may further promote the suspension and subsequent settling of fine particles, contributing to the formation of EM2 near the glacier front (Hass et al., 2010; Ahn et al., 2024). On the other hand, EM3, which contains both fine and coarse particles, appeared exclusively in the middle core 1161MUC, located at the central site of Kongsfjorden. This distribution is consistent with the presence of rivers and streams in Kongsfjorden, which are mainly concentrated in the middle part of the fjord. River systems, such as those connected to land-terminating glaciers—including the Bayelva River near Ny-Ålesund—transport both sediment and organic carbon inputs into the fjord (D'Angelo et al., 2018; Husum et al., 2019), contributing to the deposition of both fine and coarse particles in the middle region of the fjord.

### 4.2 Source of sedimentary organic carbon: bulk parameters

https://doi.org/10.5194/egusphere-2025-957
Preprint. Discussion started: 12 March 2025


The TOC values of the three sediment cores varied significantly along Kongsfjorden, with the innermost core 1058MUC having the lowest TOC (mean 0.3 ± 0.0 wt.%), and the outermost core 1159MUC the highest (mean 2.2 ± 0.2 wt.%) (Fig. 4). This variation was also reflected in the TOC/SA ratio (Figs. 7A-7B), which indicates OC loading and serves as a measure of OC preservation efficiency (Keil et al., 1994; Mayer et al., 1994; Stein et al., 2004; Zonneveld et al., 1997). Values between 0.4 and 1.0 suggest a balance between OC supply and degradation (Keil et al., 1997). However, values below 0.4, are observed in the innermost core. In Kongsfjorden, D'Angelo et al. (2018) reported that lithogenic material accounted for the dominant sediment fraction (64–78%), and Svendsen et al. (2002) highlighted significant deposition of mineral material in the inner fjord. Therefore, the lower OC loading in the innermost core 1058MUC is likely attributed to the deposition of coarse-grained terrestrial minerals (see Fig. 6B) that dilute the OC content. In contrast, higher OC loading in the middle and outer cores, with values greater than 1.0, suggests enhanced OC preservation efficiency, likely due to adsorption onto fine-grained minerals (see Fig. 6B) that reduce degradation (Keil et al., 1994; Mayer, 1994; Blair and Aller, 2012).

Similar to the TOC, the $N_{tot}$ and $N_{org}$ values were higher in the outermost core 1159MUC compared to the middle and innermost cores 1161MUC and 1058MUC (Fig. 7C, see also Fig. 4). The TOC and N (both $N_{tot}$ and $N_{org}$) contents in all three cores largely overlapped with those of surface sediments from Kongsfjorden and Krossfjorden (Kim et al., 2023 and references therein). In contrast, small drifted ice containing IRD samples from Kongsfjorden and Krossfjorden had lower TOC and $N_{tot}$ contents than the three core sediments, while coal samples from Kongsfjorden exhibited significantly higher TOC and $N_{tot}$ levels. The $N_{tot}$/TOC and $N_{org}$/TOC ratios were also highest in the outermost core (Fig. 7D, see also Fig. 4). Additionally, the $\delta^{13}C_{org}$ values were more enriched in the outermost core (Fig. 7D, see also Fig. 4), suggesting an increased contribution of marine OC to sedimentary OC towards the outer fjord. Notably, the $\delta^{13}C_{org}$ values of the three cores fell within the range of those observed in the small drifted ice containing IRD and coal samples, as well as the surface sediments from Kongsfjorden. However, the $\delta^{13}C_{org}$ values of most surface sediments and small drifted ice containing IRD samples from Krossfjorden were higher than those from Kongsfjorden, generally falling outside the range observed in all three cores. This difference may be associated with the Quaternary marine deposits exposed in Krossfjorden (Fig. S6, Dallmann and Elvevold, 2015), which could supply older, $^{13}C$-enriched marine-derived OC. These observations suggest that the

https://doi.org/10.5194/egusphere-2025-957
Preprint. Discussion started: 12 March 2025


contribution of Krossfjorden to sedimentary OC in all three cores was minimal. The $\Delta^{14}C_{org}$ values of the innermost core (1058MUC) were more depleted than those of the other two cores (Figs. 7E-7F). Similarly, small drifted ice containing IRD and surface sediment samples collected near the marine-terminating glacier front in Kongsfjorden exhibited similarly depleted values. Notably, the $\Delta^{14}C_{org}$ values of the other two cores fell between those of the glacier-front samples and those from the outer fjord. These results align with Kim et al. (2023), who suggested that the significant depletion of $\Delta^{14}C_{org}$ in the surface sediments of Svalbard fjords indicates that recently fixed terrestrial and marine OC alone cannot account for the sedimentary OC. Instead, a substantial amount of old OC, likely from petrogenic and soil-derived sources, contributes to the sedimentary OC in Kongsfjorden.

The relationship between TOC and mean grain size showed no clear correlation, with the sediments predominantly consisting of silt fractions (Fig. S7A). Similarly, TOC content did not exhibit a distinct relationship with sediment sorting values (Fig. S7B). The sediments were generally poorly sorted, with a high silt content, a characteristic feature of glacial environments where deposits are incompletely sorted due to the indiscriminate nature of glacial transport (Singh et al., 2019). The poor sorting observed across all morphological zones highlights fluctuating energy conditions during deposition, likely driven by episodic glacial advances and retreats. These variations suggest that the prevailing climatic conditions in Kongsfjorden were neither stable nor persistent over extended periods. Overall, the sedimentary characteristics of Kongsfjorden indicate a fjord environment significantly influenced by glacial input. The repeated cycles of glacial advance and retreat have resulted in the accumulation of sediments with varied grain sizes and sorting patterns, reflecting the dynamic and complex interplay between terrestrial and marine OC processes within this glaciated fjord system.

### 4.3 Source of sedimentary organic carbon: lignin phenol parameters

In a previous study conducted in Svalbard fjords, Kim et al. (2023) defined two OC components (petrogenic OC and biogenic OC) to identify the source of $^{14}C$-depleted OC in sedimentary OC. To further investigate the contributions of biogenic OC sources to Kongsfjorden, we analyzed lignin phenols obtained through alkaline CuO oxidation. Lignin phenols serve as valuable terrestrial biomarkers because they are exclusively

https://doi.org/10.5194/egusphere-2025-957
Preprint. Discussion started: 12 March 2025


synthesized by terrestrial higher plants (Hedges and Mann, 1979; Goñi et al., 2005). The ratios of S/V and C/V are used to evaluate the relative contributions of four components: non-woody angiosperms, woody angiosperms, non-woody gymnosperms, and woody gymnosperms (Hedges and Mann, 1979; Goñi and Hedges, 1995). In the three Kongsfjorden cores, lignin phenols primarily consisted of a mixture of non-woody gymnosperm OC with inputs from gymnosperm wood-derived tissues, along with some contributions from non-woody angiosperms, consistent with previous studies (Fig. 8A). Lignin phenol concentrations were highest in the innermost core 1058MUC, compared to the other two cores (Fig. 8B; see also Fig. 5). These values fell within the range observed in surface sediments from Svalbard fjords, including Kongsfjorden and Krossfjorden (Figs. S8A and S9A).

3,5-Bd is primarily produced during soil degradation processes, leading to its enrichment in soils (e.g., Prahl et al., 1994; Goñi et al., 2000; Houel et al., 2006; Otto and Simpson, 2006). As a result, the 3,5-Bd/V ratio is widely used to assess the extent of lignin degradation and to trace inputs of soil-derived OC to aquatic systems (e.g., Prahl et al., 1994; Goñi et al., 2000; Houel et al., 2006; Otto and Simpson, 2006). Similarly, the (Ad/Al)v ratio reflects lignin oxidation, as the conversion of aldehyde functional groups into acidic phenols through propyl side-chain modification serves as a key indicator of lignin degradation in sedimentary organic matter (e.g., Hedges and Ertel, 1982; Goñi and Hedges, 1992; Otto and Simpson, 2006). The (Ad/Al)v ratios below 0.3 typically indicate relatively fresh vascular plant detritus, whereas values exceeding 0.5 are generally associated with extensively altered soils with significantly depleted $^{14}C$ signatures (e.g., Hedges and Ertel, 1982; Goñi and Hedges, 1992; Otto and Simpson, 2006). Among the three cores, both 3,5-Bd/V and (Ad/Al)v ratios were lowest in the innermost core 1058MUC (Figs. 8C and 8D, see also Fig. 5). Notably, coal samples also exhibited relatively low values, averaging 0.48 for the 3,5-Bd/V ratio and 0.49 for the (Ad/Al)v ratio, similar to those of the innermost core 1058MUC. Both the 3,5-Bd/V and (Ad/Al)v ratios were higher in the outermost core 1159MUC than in the middle and innermost cores 1161MUC and 1058MUC, suggesting an increased contribution of degraded terrestrial OC to sedimentary OC with increasing distance offshore. Notably, the differences among the three core sites were smaller for the (Ad/Al)v ratio than for the 3,5-Bd/V ratio.

Previously, Kim et al. (2023) suggested that biogenic OC includes not only recently fixed terrestrial and marine biomass but also pre-aged OC from soils, which can be

https://doi.org/10.5194/egusphere-2025-957
Preprint. Discussion started: 12 March 2025


transported to fjords through glacial erosion and surface runoff. Therefore, we examined the lignin phenol concentrations and (Ad/Al)v ratios of these biogenic OC sources—plant-derived, soil-derived, and marine OC (Fig. S8). Most core sediments exhibited lower lignin phenol concentrations and (Ad/Al)v ratios compared to the average values of soils collected in the Ny-Ålesund and Longyearbyen regions. Thus, the soil values encompass the range observed in all three cores and most surface sediments collected in Svalbard fjords. However, surface sediments from Krossfjorden exhibited distinct (Ad/Al)v ratios and $\delta^{13}C_{org}$ values, which fell outside the soil range. This difference may result from the complex bedrock types present in Svalbard fjords (Fig. S6), which can influence OC characteristics (Kim et al., 2023). These findings suggest that the contribution of Krossfjorden to the sedimentary OC in all three cores was limited.

### 4.4 Four OC source apportionments

In this study, we adopted the OC source classification concept from the surface sediment study in Svalbard fjords (Kim et al., 2023) and defined four distinct sedimentary OC sources: petrogenic, soil-derived, plant-derived, and marine OC. To estimate the relative proportions of these OC sources, we applied a four-source apportionment approach based on $\Delta^{14}C_{org}$, $\delta^{13}C_{org}$, and lignin parameters such as the (Ad/Al)v ratio and lignin phenol concentrations, using a Monte Carlo (MC) analysis. End-member values for each OC source, as reported in Kim et al. (2023) (Table S5), were used in the analysis.

Firstly, similar to the previous study by Kim et al. (2023), the relative proportions of the four OC sources were calculated using Method 1, based on $\Delta^{14}C_{org}$, $\delta^{13}C_{org}$, and the (Ad/Al)v ratio (Fig. 9). The petrogenic OC fraction was the highest in core 1058MUC, located at the innermost site, ranging from 72.6% to 82.2%. This was followed by core 1161MUC, which ranged from 35.6% to 52.2%, and core 1159MUC, which ranged from 30.1% to 42.7%. Marine OC fractions were highest in core 1159MUC at the outermost site, ranging from 34.0% to 52.0%, followed by core 1161MUC at 26.8% to 52.0%, and core 1058MUC at 10.4% to 26.0%.

Secondly, we calculated the relative proportions of the four OC sources using Method 2, which is based on $\Delta^{14}C_{org}$, $\delta^{13}C_{org}$, and lignin phenol concentrations. This method was chosen because previous studies used lignin phenol concentrations for source mixing models, assuming a value of 0 for marine phytoplankton (Tesi et al., 2016; Pempkowiak et al., 2020). To validate this approach, we first applied Method 2 to surface sediments previously investigated by Kim et al. (2023). Overall, the estimated relative

https://doi.org/10.5194/egusphere-2025-957
Preprint. Discussion started: 12 March 2025


contributions of the four OC sources were within a similar range to those reported in the earlier study, and the spatial distribution pattern exhibited similar trends between both approaches (Fig. S10). For the three sediment cores in this study, the results from Method 2 also were consistent with those from Method 1. Petrogenic OC fractions were highest in core 1058MUC, located at the innermost site (mean 79.2 ± 3.3%), followed by cores 1161MUC (mean 46.6 ± 4.4%) and 1159MUC (mean 40.7 ± 1.7%) (Fig. 9). In contrast, marine OC fractions were highest in core 1159MUC, located at the outermost site (mean 50.4 ± 4.7%), followed by core 1161MUC (mean 42.9 ± 5.2%) and core 1058MUC (mean 16.5 ± 3.2%). These findings suggest that Method 2 did not significantly alter the trends observed from Method 1. However, it is important to note that some surface sediments from Kongsfjorden and Krossfjorden exhibited (Ad/Al)v ratios outside the range of soil values (Fig. S9B). In contrast, the lignin phenol concentration data were well within the expected range for soils (Fig. S9A). Given this, Method 2 appears to be a more appropriate approach than Method 1 for assessing the relative proportions of the four OC sources in the Svalbard fjords.

Nonetheless, both methods showed that the plant-derived OC fraction contributed minimally compared to the dominant sources, such as petrogenic and marine OC. However, soil-derived OC contributions were higher in the middle and outermost cores 1161MUC and 1159MUC than in the innermost core 1058MUC, suggesting a specific input of soil-derived OC in the middle part of the fjord, likely due to terrestrial contributions from surface runoff. Supporting evidence for this is the presence of EM3 in core 1161MUC (Fig. 6B), which indicates significant river input of both fine and coarse particles to this part of the fjord, a feature not observed in the other two cores.

### 4.5 Potential future implication on carbon dynamics

The accumulation rates (AR) of each OC source in the sediment cores were calculated to investigate OC fluxes over recent timescales. Wet bulk density (WBD) and porosity (PO) were determined using the water content and dry bulk density of the samples, as described by Hamilton (1971). The AR was calculated based on the sedimentation rate (SR), WBD, and PO of each sample, as follows (cf. Gealy, 1971):

$$AR\left(\frac{g/cm^2}{yr}\right) = \mathrm{SR} \times \left[WBD - 1.025 \times \left(\frac{PO}{100}\right)\right] \quad (2)$$

https://doi.org/10.5194/egusphere-2025-957
Preprint. Discussion started: 12 March 2025


As the next step, the ARs of bulk OC were calculated using Equation 2, as follows (cf. Nam, 1997):

$$\text{Bulk OC AR} = (\text{TOC of sediment sample}/100) \times \text{AR} \quad (3)$$

The ARs of petrogenic, soil-derived, plant-derived, and marine OC were calculated from bulk OC AR using Equation 3, as follows:

$$\text{AR of each OC source} = (\text{each OC source fraction}/100) \times \text{bulk OC AR} \quad (4)$$

The bulk OC AR was 0.47 ± 0.06 g/cm²/yr at the middle site (core 1161MUC), higher than the outermost site (core 1159MUC), which had a value of 0.26 ± 0.03 g/cm²/yr (data not shown). The ARs of the four OC sources, determined by both Methods 1 and 2, are presented in Fig. 10. For core 1161MUC, petrogenic OC ARs were similar between Method 1 (0.18 ± 0.03 g/cm²/yr) and Method 2 (0.18 ± 0.02 g/cm²/yr). Among biogenic sources, marine OC had the highest ARs (0.15 ± 0.03 g/cm²/yr for Method 1; 0.17 ± 0.03 g/cm²/yr for Method 2), two to four times higher than soil-derived OC and 20–70 times higher than plant-derived OC. Similarly, for core 1159MUC, petrogenic OC ARs were consistent across both methods (0.05 ± 0.01 g/cm²/yr), with marine OC showing the highest biogenic ARs (0.05 ± 0.01 g/cm²/yr for Method 1; 0.06 ± 0.01 g/cm²/yr for Method 2), exceeding those of soil-derived and plant-derived OC.

For all petrogenic and biogenic OC sources, ARs were higher at the middle site (core 1161MUC) compared to the outermost site (core 1159MUC) (Fig. 10). Notably, marine OC ARs at core 1161MUC showed an increasing trend since approximately the 1970s, while petrogenic OC ARs decreased over the same period. In contrast, no clear trends were observed for either petrogenic or marine OC ARs at the outermost site (core 1159MUC) (see also Fig. S11). Interestingly, the increase in marine OC ARs at the middle site since the 1970s (Fig. 11A) coincides with shifts in sediment composition, characterized by increasing relative abundances of EM1b (Fig. 11B). This pattern suggests an intensification of meltwater discharge from marine-terminating glaciers. The rise in marine OC ARs also coincides with broader climatic and environmental changes in the Svalbard region. Since the 1970s, surface air temperatures in Ny-Ålesund have increased at a rate four times faster than the global average from 1975 to 2014 (Fig. 11C,

https://doi.org/10.5194/egusphere-2025-957
Preprint. Discussion started: 12 March 2025


Wei et al., 2016). Concurrently, the Barents Sea summer sea ice extent has declined rapidly (Fig. 11D, NSIDC; National Snow and Ice Data Center, http://nsidc.org/data/seaice_index), and the Blomstrandbreen glacier has experienced significant retreat (Fig. 11D, Burton et al., 2016). These changes suggest a strong link between climate warming and shifts in Kongsfjorden's carbon dynamics. Notably, during the same period, integrated temperatures (50 to 300 m water depth) from the transect across 78°N, in the core of the WSC in western Svalbard, also showed an increasing trend (Fig. 11C, Tesi et al., 2021). This suggests a connection between the observed warming of AW and broader regional climatic and environmental changes. Longer-term environmental reconstructions support this connection, with studies reporting increased AW inflow and associated productivity in Kongsfjorden in the early 20th century (Husum et al., 2019; Tesi et al., 2021). Ingrosso et al. (2025) also documented rapid greening of western Svalbard during the same period, which they attributed to extremely low sea ice extent, driven primarily by the strong advection of warm AW into Arctic fjords. This historical context highlights the likely influence of enhanced AW inflow on the rise in marine OC ARs recorded at the middle site (core 1161MUC) since the 1970s, with increased marine productivity and OC burial contributing to this rise while driving the concurrent decline in petrogenic OC ARs.

## 5. Conclusions

In this study, we investigated three multicores collected from Kongsfjorden, Svalbard, to explore the spatial and temporal dynamics of sedimentary OC over recent centuries. Bulk parameter analyses indicate that Kongsfjorden was the primary source of OC in the sediments, with minor contributions from Krossfjorden. Additionally, a substantial amount of old OC, likely derived from petrogenic and soil sources, was present in the sedimentary OC in Kongsfjorden. To estimate the relative proportions of OC sources, we applied a four-source apportionment approach based on $\Delta^{14}C_{org}$, $\delta^{13}C_{org}$, and lignin parameters, including the (Ad/Al)v ratio and lignin phenol concentrations, using MC analysis. Our results revealed that petrogenic OC fractions were highest at the innermost site, while marine OC fractions dominated at the outermost site. The plant-derived OC fraction contributed minimally compared to petrogenic and marine OC, while soil-derived OC was more substantial at the middle and outermost sites, suggesting enhanced input from surface runoff. For all OC sources, ARs were higher at the middle site than at the outermost site. Notably, marine OC ARs at the middle site showed an

https://doi.org/10.5194/egusphere-2025-957
Preprint. Discussion started: 12 March 2025


increasing trend since approximately the 1970s, likely reflecting enhanced AW inflow, which boosted marine productivity and OC burial. These findings underscore the significant role of AW inflow in reshaping carbon dynamics in Svalbard fjords over the past few decades and highlight the sensitivity of Arctic fjords to climate shifts. More importantly, our study suggests that the abrupt AW increases during the 20th century followed a two-step process, driven by complex and yet-to-be-fully-understood mechanisms. Future research should prioritize high-resolution climate modeling for the Svalbard region to better constrain the timing, causes, and impacts of AW changes, ultimately refining predictions of climate and carbon cycle dynamics in the rapidly warming Arctic. Given their role as critical OC reservoirs, Arctic fjords may function as both sources and sinks of carbon in a warming climate, emphasizing the need for further research to assess the long-term consequences of climate-induced changes on regional carbon cycling.

**Data availability**

All the primary data are presented in the Supplement. The other data are available upon request to the corresponding author (Jung-Hyun Kim, jhkim123@kopri.re.kr).

**Supplement**

The supplement related to this article is available online at Korea Polar Data Center (http://dx.doi.org/doi:10.XXXXX/KOPRI-KPDC-XXXXX).

**Author contributions**

D.K. and J.-H.K. designed the study, interpreted the majority of the data, and wrote the manuscript. Y.K.A., M.F., and S.I.N. contributed to sample acquisition. D.K. conducted the biomarker analyses, while Y.K.A. performed the grain size analyses and the end-member modeling. All authors commented on the manuscript and contributed to its revision.

**Competing interest**

The authors declare that they have no conflict of interest.

**Acknowledgements**

https://doi.org/10.5194/egusphere-2025-957
Preprint. Discussion started: 12 March 2025


We thank the captains and crews of R/V *Helmer Hanssen* for their support at sea during sediment core retrievals. We also extend our gratitude to Y. Son and Y. Joe for their analytical assistance in the laboratory at KOPRI.

**Financial support**

This study was fully supported by grants from the National Research Foundation of Korea (NRF), funded by the Ministry of Science and ICT (NRF-2021M1A5A1075512).

**References**

Ahn, Y., Joe, Y. J., Jang, K., Kim, J.-H., Son, Y. J., Forwick, M., Hong, S., Nam, S.-I.: Post-glaciation depositional changes in Wijdefjorden, northern Svalbard, using grain-size end-member modelling. Mar. Geol., 472, 107306, https://doi.org/10.1016/j.margeo.2024.107306, 2024.

Appleby, P. G.: Dating recent sediments by 210 Pb: problems and solutions. Seminar on Dating of sediments and determination of sedimentation rate, pp p. 7–24, https://inis.iaea.org/records/vtsmx-fvz88, 1998.

Appleby, P. G., Oldfield, F.: The calculation of lead-210 dates assuming a constant rate of supply of unsupported $^{210}$Pb to the sediment. Catena, 5, 1–8, https://doi.org/10.1016/S0341-8162(78)80002-2, 1978.

Årthun, M., Eldevik, T., Smedsrud, L., Skagseth, O., Ingvaldsen, R.: Quantifying the influence of Atlantic heat on Barents Sea ice variability and retreat, J. Clim., 25, 4736–4743, http://doi.org/10.1175/JCLI-D-11-00466.1, 2012.

Bianchi, T. S., Cui, X., Blair, N. E., Burdige, D. J., Eglinton, T. I., Galy, V.: Centers of organic carbon burial and oxidation at the land-ocean interface, Org. Geochem., 115, 138–155, https://doi.org/10.1016/j.orggeochem.2017.09.008, 2017.

Bianchi, T. S., Cui, X., Blair, N. E.: Fjords as aquatic critical zones (ACZs), Earth Sci. Rev., 203, 103145, https://doi.org/10.1016/j.earscirev.2020.103145, 2020.

Blair, N. E., & Aller, R. C.: The fate of terrestrial organic carbon in the marine environment. Annu. Rev. Mar. Sci., 4, 401–423, https://doi.org/10.1146/annurev-marine-120709-142717, 2012.

Brogi, S. R., Jung, J. Y., Ha, S.-Y., & Hur, J.: Seasonal differences in dissolved organic matter properties and sources in an Arctic fjord: Implications for future conditions, Sci. Total Environ., 694, 133740, https://doi.org/10.1016/j.scitotenv.2019.133740, 2019.

https://doi.org/10.5194/egusphere-2025-957
Preprint. Discussion started: 12 March 2025


643 Burton, D. J., Dowdeswell, J. A., Hogan, K. A., Noormets, R.: Marginal fluctuations of a
644 Svalbard surge-type tidewater glacier, Blomstrandbreen, since the Little Ice Age:
645 A record of three surges, Arctic, Antarctic, and Alpine Research, 48, 411–426,
646 http://doi.org/10.1657/AAAR0014-094, 2016.
647 Choudhary, S., Neelavanan, K., Saalim, S. M.: Microplastics in the surface sediments of
648 Krossfjord-Kongsfjord system, Svalbard, Arctic, Mar. Pollut. Bull., 176, 113452,
649 http://doi.org/10.1016/j.marpolbul.2022.113452, 2022.
650 Cottier, F. R., Nilsen, F., Inall, M. E., Gerland, S., Tverberg, V., Svendsen, H.: Wintertime
651 warming of an Arctic shelf in response to large-scale atmospheric circulation,
652 Geophys. Res. Lett., 34, L10607, http://doi.org/10.1029/2007GL029948, 2007.
653 D'Angelo, A., Giglio, F., Miserocchi, S., Sanchez-Vidal, A., Aliani, S., Tesi, T.: Multi-
654 year particle fluxes in Kongsfjorden, Svalbard, Biogeosciences, 15, 5343–5363,
655 https://doi.org/10.5194/bg-15-5343-2018, 2018.
656 Dahlke, F. T., Wohlrab, S., Butzin, M., Pörtner, H.-O.: Thermal bottlenecks in the life
657 cycle define climate vulnerability of fish, Sciences, 369, 65–70,
658 http://doi.org/10.1126/science.aaz3658, 2020.
659 Dallmann, W. K., Elvevold, S.: Bedrock geology. Geoscience Atlas of Svalbard, Re-port
660 Series 148, Norsk Polarinstitutt, Tromsø, pp.133–173,
661 http://hdl.handle.net/11250/2580810, 2015.
662 De Rovere, F., Langone, L., Schroeder, K., Miserocchi, S., Giglio, F., Aliani, S., &
663 Chiggiato, J.: Water masses variability in inner Kongsfjorden (Svalbard) during
664 2010–2020, Front. Mar. Sci., 9, 741075,
665 https://doi.org/10.3389/fmars.2022.741075, 2022.
666 Elverhøi, A., Liestøl, O. & Nagy, J.: Glacial erosion, sedimentation and microfauna in
667 the inner part of Kongsfjorden, Spitsbergen, Norsk Polarinstitutt Skrifter, 172, 33–
668 58, http:// core.ac.uk/reader/30910780#page=35, 1980.
669 Forwick, M., Vorren, T. O.: Late Weichselian and Holocene sedimentary environments
670 and ice rafting in Isfjorden, Spitsbergen, Palaeogeogr. Palaeoclimatol. Palaeoecol.,
671 280, 258–274, http://doi.org/10.1016/j.palaeo.2009.06.026, 2009.
672 Friedlingstein, P., et al.: Global carbon budget 2020, Earth Syst. Sci. Data, 12, 3269–3340,
673 http://doi.org/10.5194/essd-12-3269-2020, 2020.
674 Gealy, E. L. : Saturated bulk density, grain density, and porosity of sediment cores from
675 the western equatorial Pacific: Leg 7, Glomar Challenger. Initial Reports of the
676 Deep Sea Drilling Project, 7, 1081–1104, 1971.

https://doi.org/10.5194/egusphere-2025-957
Preprint. Discussion started: 12 March 2025


677 Goñi, M. A., & Hedges, J. I. : Lignin dimers: structures, distribution, and potential
678 geochemical applications, Geochim. Cosmochim. Acta, 56, 4025–4043,
679 https://doi.org/10.1016/0016-7037(92)90014-A, 1992.
680 Goñi, M. A., & Hedges, J. I. : Sources and reactivities of marine-derived organic matter
681 in coastal sediments as determined by alkaline CuO oxidation, Geochim.
682 Cosmochim. Acta, 59, 2965–2981, https://doi.org/10.1016/0016-7037(95)00188-3,
683 1995.
684 Goñi, M. A., Yunker, M. B., MacDonald, R. W., & Eglinton, T. I.:. Distribution and
685 sources of organic biomarkers in arctic sediments from the Mackenzie River and
686 Beaufort Shelf, Mar. Chem., 71, 23–51, https://doi.org/10.1016/S0304-
687 4203(00)00037-2, 2000.
688 Goñi, M. A., Yunker, M. B., MacDonald, R. W., & Eglinton, T. I.: The supply and
689 preservation of ancient and modern components of organic carbon in the Canadian
690 Beaufort Shelf of the Arctic Ocean, Mar. Chem., 93, 53–73,
691 https://doi.org/10.1016/j.marchem.2004.08.001, 2005.
692 Hamilton, E. L.1971 Elastic properties of marine sediments, J. Geophys. Res., 76, 293–
693 635, https://doi.org/10.1190/1.1440168, 1971.
694 Hass, H. C., Kuhn, G., Monien, P., Brumsack, H.-J., Forwick, M.: Climate fluctuations
695 during the past two millennia as recorded in sediments from Maxwell Bay, Wouth
696 Shetland Islands, West Antarctica, Fjord Systems and Archives, 344,
697 http://doi.org/10.1144/SP344, 2010.
698 Hedges, J. I., & Ertel, J. R.: Characterization of lignin by gas capillary chromatography
699 of cupric oxide oxidation products, Anal. Chem., 54, 174–178,
700 https://doi.org/10.1021/ac00239a007, 1982.
701 Hedges, J. I., & Mann, D. C.: The characterization of plant tissues by their lignin
702 oxidation products, Geochim. Cosmochim. Acta, 43, 1803–1807,
703 https://doi.org/10.1016/0016-7037(79)90028-0, 1979.
704 Herzke, D., Ghaffari, P., Sundet, J. H., Tranang, C. A., Halsband, C.: Microplastic fiber
705 emissions from wastewater effluents: abundance, transport behavior and exposure
706 risk for biota in an Arctic Fjord, Front. Environ. Sci., 9, 662168,
707 http://doi.org/10.3389/fenvs.2021.662168, 2021.
708 Houel, S., Louchouarn, P., Lucotte, M., Canuel, R., & Ghaleb, B.: Translocation of soil
709 organic matter following reservoir impoundment in boreal systems: Implications

https://doi.org/10.5194/egusphere-2025-957
Preprint. Discussion started: 12 March 2025


for in situ productivity, Limnol. Oceanogra., 51, 1497–1513, https://doi.org/10.4319/lo.2006.51.3.1497, 2006.

Husum, K., et al.: The marine sedimentary environments of Kongsfjorden, Svalbard: An archive of polar environmental change, Polar Res., 38, 3380, https://doi.org/10.33265/polar.v38.3380, 2019.

Ingrosso, G., Ceccarelli, C., Giglio, F., Giordano, P., Hefter, J., Langone, L., Miserocchi, S., Mollenhauer, G., Nogarotto, A., Sabino, M., Tesi, T.: Greening of Svalbard in the twentieth century driven by sea ice loss and glaciers retreat, Commun. Earth Environ., 6, 30, http://doi.org/10.1038/s43247-025-01994-y, 2025.

Ito, H., and S. Kudoh,: Characteristics of water in Kongsfjorden, Svalbard, Proc. NIPR Symp. Polar Meteorol. Glaciol., 11, 211–232, 1997.

Jernas, P., et al.: Annual changes in Arctic fjord environment and modern benthic foraminiferal fauna: Evidence from Kongsfjorden, Svalbard, Global Planet. Change, 163, 119–140, 2018.

Jordà-Molina, È., Renaud, P. E., Silberberger, M. J., Sen, A., Bluhm, B. A., Carroll, M. L., Ambrose Jr., W. G., Cottier, F., Reiss, H.: Seafloor warm water temperature anomalies impact benthic macrofauna communities of a high-Arctic cold-water fjord. Mar. Envrion. Res., 189. 106046, http://doi.org/10.1016/j.marenvres.2023.106046, 2023.

Keil, R. G., E. Tsamakis, C. B. Fuh, J. C. Giddings, and J. I. Hedges,:Mineralogical and textural controls on the organic composition of coastal marine sediments: Hydrodynamic separation using SPLITT-fractionation, Geochim. Cosmochim. Acta, 58, 879–893, https://doi.org/10.1016/0016-7037(94)90512-6, 1994.

Keil, R. G., L. M. Mayer, P. D. Quay, J. E. Richey, and J. I. Hedges,: Loss of organic matter from riverine particles in deltas, Geochim. Cosmochim. Acta, 61, 1507–1511, https://doi.org/10.1016/S0016-7037(97)00044-6, 1997.

Kim, J.-H., Peterse, F., Willmott, V., Klitgaard Kristensen, D., Baas, M., Schouten, S., Sinninghe Damsté, J.S.: Large ancient organic matter contributions to Arctic marine sediments (Svalbard), Limnol. Oceanogr., 56, 1463–1474, http://doi.org/10.4319/1o.2011.56.4.1463, 2011.

Kim, D., Kim, J.-H., Tesi, T., Kang, S., Nogarotto, A., Park, K., Lee, D.-H., Jin, Y.K., Shin, K.-H., Nam, S.-I.: Changes in the burial efficiency and composition of terrestrial organic carbon along the Mackenzie Trough in the Beaufort Sea, Estuar. Coastal Shelf Sci., 275, 107997, https://doi.org/10.1016/j.ecss.2022.107997, 2022.

https://doi.org/10.5194/egusphere-2025-957
Preprint. Discussion started: 12 March 2025


744 Kim, D., Kim, J.-H., Ahn, Y., Jang, K., Jung, J. Y., Bae, M., Nam, S.-I.: Large
745 contributions of petrogenic and aged soil-derived organic carbon to Arctic fjord
746 sediments in Svalbard, Sci. Rep., 13, 17935, https://doi.org/10.1038/s41598-023-
747 45141-z, 2023.
748 Knies, J., Martinez, P.: Organic matter sedimentation in the western Barents Sea region:
749 Terrestrial and marine contribution based on isotopic composition and organic
750 nitrogen content. Nor. J. Geol., 89, 79–89, 2009.
751 Knies, J., Brookes, S. & Schubert, C. J.: Re-assessing the nitrogen signal in continental
752 margin sediments: New insights from the high northern latitudes, Earth Planet. Sci.
753 Lett., 253, 471–484, http://doi.org/10.1016/j.epsl.2006.11.008, 2007.
754 Krajewska, M., Szymczak-Zyla, M., Tylmann, W., Kowalewska, G.: Climate change
755 impact on primary production and phytoplankton taxonomy in Western Spitsbergen
756 fjords based on pigments in sediments, Global Planet. Change, 189, 103158,
757 http://doi.org/10.1016/j.gloplacha.2020.103158, 2020.
758 Kumar, V., Tiwari, M., Nagoji, S., Tripathi, S.: Evidence of anomalously low $\delta^{13}C$ of
759 marine organic matter in an Arctic Fjord, Sci. Rep., 6, 36192,
760 http://10.1038/srep36192, 2016.
761 Lind, S., Ingvaldsen, R. B., Furevik, T.: Arctic warming hotspot in the northern Barents
762 Sea linked to declining sea-ice import, Nat. Clim. Change, 8, 634–639, 2018.
763 Mayer, L. M.: Surface area control of organic carbon accumulation in continental shelf
764 sediments, Geochim. Cosmochim. Acta, 58, 1271–1284,
765 https://doi.org/10.1016/0016-7037(94)90381-6, 1994.
766 McGovern, M., K. Borgå, E. Heimstad, A. Ruus, G. Christensen, and Evenset, A.: Small
767 Arctic rivers transport legacy contaminants from thawing catchments to coastal
768 areas in Kongsfjorden, Svalbard, Environ. Pollut., 304, 119191,
769 https://doi.org/10.1016/j.envpol.2022.119191, 2022.
770 Meslard, F., Bourrin, F., Many, G., Kerherve, P.: Suspended particle dynamics and fluxes
771 in an Arctic fjord (Kongsfjorden, Svalbard), Estuar. Coast. Shelf Sci., 204, 212–
772 224, http://doi.org/10.1016/j.ecss.2018.02.020, 2018.
773 Nam, S.-I.: Late Quaternary glacial history and paleoceanographic reconstructions along
774 the East Greenland continental marine: evidence from high-resolution records of
775 stable isotopes and ice-rafted debris, Rep. Polar Res., 241, pp. 21, 1997.
776 Nuth, C., Kohler, J., Konig, M., von Deschwanden, A., Hagen, J. O., Kaab, A., Moholdt,
777 G., Pettersson, R.: Decadal changes from a multi-temporal glacier inventory of

https://doi.org/10.5194/egusphere-2025-957
Preprint. Discussion started: 12 March 2025


Svalbard. The Cryosphere, 7, 1603–1621, http://doi.org/10.5194/tc-7-1603-2013, 2013.

Ó Cofaigh, C., Dowdeswell, J. A.: Laminated sediments in glacimarine environments: diagnostic criteria for their interpretation, Quat. Sci. Rev., 20, 1411–1436, http://doi.org/10.1016/S0277-3791(00)00177-3, 2001.

Otto, A., and Simpson, M. J.: Evaluation of CuO oxidation parameters for determining the source and stage of lignin degradation in soil, Biogeochem., 80, 121–142, https://doi.org/10.1007/s10533-006-9014-x, 2006.

Pempkowiak, J.: Limitation of lignin derivatives as biomarkers of land derived organic matter in the coastal marine sediments, Oceanologia, 62, 374–386, http://doi.org/10.1016/j.oceano.2020.04.004, 2020.

Polyakov, I. V., Pnyushkov, A. V., Alkire, M. B., Ashik, I. M., Baumann, T. M., Carmack, E. C., Goszczko, I., Guthrie, J., Ivanov, V. V., Kanzow, T., Krishfield, R., Kwok, R., Sundfjord, A., Morison, J., Remember, R., Yulin, A.: Greater role for Atlantic inflows on sea-ice loss in the Eurasian Basin of the Arctic Ocean, Science, 356, 285–291, 2017.

Prahl, F. G., Ertel, J. R., Goñi, M. A., Sparrow, M. A., Eversmeyer, B.: Terrestrial organic carbon contributions to sediments on the Washington margin, Geochim. Cosmochim. Acta, 58, 3035–3048, https://doi.org/10.1016/0016-7037(94)90177-5, 1994.

Pramanik, A., Kohler, J., Lindback, K., How, P., Van Pelt, W., Liston, G., Schuler, T. V.: Hydrology and runoff routing of glacierized drainage basins in the Kongsfjord area, northwest Svalbard, The Cryosphere, http://doi.org/10.5174/tc-2020-197, 2020.

Rantanen, M., Karpechko, A. Y., Lipponen, A., Nordling, K., Hyvärinen, O., Ruosteenoja, K., Räisänen, J.: The Arctic has warmed nearly four times faster than the globe since 1979, Commun. Earth Environ., 3, 168, https://doi.org/10.1038/s43247-022-00498-3, 2022.

Saloranta, T. M., Svendsen, H.: Across the Arctic front west of Spitsbergen: high-resolution CTD sections from 1998–2000, Polar Research, 20, 177–184, http://doi.org/10.3402/polar.v20i2.6515, 2001.

Schauer, U., Fahrbach, E., Osterhus, S., Rohardt, G.: Arctic warming through the Fram Strait: Oceanic heat transport from 3 years of measurements, J. Geophys. Res. Oceans, 109, C06026, 2004.

https://doi.org/10.5194/egusphere-2025-957
Preprint. Discussion started: 12 March 2025


Singh, D. S., Dubey, C. A., Kumar, D., Vishawakarma, B., Singh, A. K., Tripathi, A., Sharma, R.: Monsoon variability and major climatic events between 25 and 0.05 ka BP using sedimentary parameters in the Gangotri glacier region, Garhwal Himalaya, India. Quater. Inter., 507, 148–155, https://doi.org/10.1016/j.quaint.2019.06.024, 2019.

Skogseth, R., Asplin, L., Budgell, W. P., Eldevik, T., Gerland, S., Haugan, P., Zamelczyk, K.: Variability and decadal trends in the Isfjorden (Svalbard) ocean climate and circulation – An indicator for climate change in the European Arctic, Progr. Oceanogr., 187, 102394, https://doi.org/10.1016/j.pocean.2020.102394, 2020.

Smith, R. W., Bianchi, T. S., Allison, M., Savage, C., Galy, V.: High rates of organic carbon burial in fjord sediments globally, Nat. Geosci., 8, 450–453, http://doi.org/10.1038/NGEO2421, 2015.

Stein, R., and MacDonald, R. W.: The organic carbon cycle in the Arctic Ocean, Springer. https://doi.org/10.1007/978-3-642-18912-8, 2004.

Stuiver, M., and Polach, H. A.: Discussion: Reporting of 14C data. Radiocarbon, 19, 355–363, https://doi.org/10.1017/S0033822200003672, 1977.

Svendsen, H., Beszczynska-Møller, A., Hagen, J. O., Lefauconnier, B., Tverberg, V., Gerland, S., Ørbæk, J. B.: The physical environment of Kongsfjorden–Krossfjorden, an Arctic fjord system in Svalbard, Polar Res., 21, 133–166, https://doi.org/10.3402/polar.v21i1.6479, 2002.

Tesi, T., Muschitiello, F., Smittenber, R. H., Jakobsson, M., Vonk, J. E., Hill, P., Andersson, A., Kirchner, N., Noormets, R., Dudarev, O., Semiletov, I., Gustafsson, Ö.: Massive remobilization of permafrost carbon during past-glacial warming, Nat. Commun., 7, 13653, http://doi.org/10.1038/ncomms13653, 2016.

Tesi, T., Muschitiello, F., Mollenhauer, G., Miserocchi, S., Langone, L., Ceccarelli, C., Panieri, G., Chiggiato, J., Nogarotto, A., Hefter, J., Ingrosso, G., Giglio, F., Giordano, P., Capotondi, L.: Rapid atlantification along the Fram Strait at the beginning of the 20th century, Sci. Advances, 7, eabj2946, http://doi.org/10.1126/sciadv.abj2946, 2021.

Torsvik, T., Albretsen, J., Sundfjord, A., Kohler, J., Sandvik, A. D., Skarohamar, J., Lindback, K., Everett, A.: Impact of tidewater glacier retreat on the fjord system: Modeling present and future circulation in Kongsfjorden, Svalbard, Estuar. Coast. Shelf Sci., 220, 152–165, http://doi.org/10.1016/j.ecss.2019.02.005, 2019.

https://doi.org/10.5194/egusphere-2025-957
Preprint. Discussion started: 12 March 2025


844 Tverberg, V., Skogseth, R., Cottier, F., Sundfjord, A., Walczowski, W., Inall, M. E., Falck,
845 E., Pavlova, O., Nilsen, F.: The Kongsfjorden transect: seasonal and inter-annual
846 variability in hydrography, The Ecosystem of Kongsfjorden, Svalbard, 49–104,
847 http://doi.org/10.1007/978-3-319-46425-1_3, 2019.
848 van Hateren, J. A., Prins, M. A., van Balen, R. T.: On the genetically meaningful
849 decomposition of grain-size distributions: A comparison of different end-member
850 modelling algorithms, Sediment. Geol., 375, 49–71,
851 http://doi.org/10.1016/j.sedgeo.2017.12.003, 2018.
852 Vorren, T. O., Hald, M., Thomsen, E.: Quaternary sediments and environments on the
853 continental shelf off northern Norway, Mar. Geol., 57, 229–257,
854 http://doi.org/10.1016/0025-3227(84)90201-9, 1984.
855 Wei, T., Ding, M., Wu, B., Lu, C., & Wang, S.: Variations in temperature-related extreme
856 events (1975–2014) in Ny-Ålesund, Svalbard, Atmos. Sci. Lett., 17, 102–108,
857 https://doi.org/10.1002/asl.632, 2016.
858 Winkelmann, D., Knies, J.: Recent distribution and accumulation of organic carbon on
859 the continental marine west off Spitsbergen, Geochem. Geophys. Geosyst., 6,
860 Q09012, http://doi.org/10.1029.2005GC000916, 2005.
861 Zaborska, A., Carroll, J., Papucci, C., Carroll, M., Walkusz-Miotk, J., & Włodarska-
862 Kowalczuk, M.: Some sediment characteristics and sedimentation rates in an Arctic
863 fjord (Kongsfjorden, Svalbard), Rocznik Ochrona Środowiska, 8, 79–96, 2006.
864 Zhu, Z.-Y., Wu, Y., Liu, S.-M., Wenger, F., Hu, J., Zhang, J., Yao, P.: Organic carbon
865 flux and particulate organic matter composition in Arctic valley glaciers: Examples
866 from the Bayelva River and adjacent Kongsfjorden, Biogeosciences, 13, 975–987,
867 https://doi.org/10.5194/bg-13-975-2016, 2016.
868 Zonneveld, K. A. F., Versteegh, G. J. M., & de Lange, G. J.: Preservation of organic-
869 walled dinoflagellate cysts in different oxygen regimes: A 10,000 years natural
870 experiment. Mar. Micropaleontol., 29, 393–405, https://doi.org/10.1016/S0377-
871 8398(96)00032-1, 1997.

https://doi.org/10.5194/egusphere-2025-957
Preprint. Discussion started: 12 March 2025


## Figures

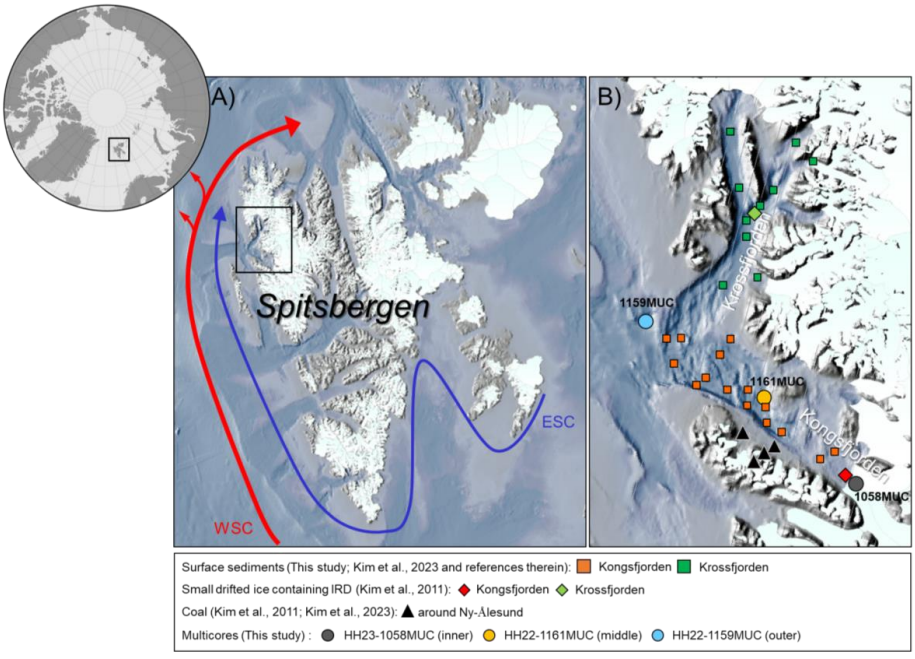


Fig. 1. Map of the study area showing (A) the Svalbard archipelago and (B) the sampling sites in Kongsfjoren and Krossfjorden considered in this study. White land areas indicate present-day glacier coverage. ESC and WSC denote East Spitsbergen Current and West Spitsbergen Current, respectively. Filled circles represent core sampling sites, while filled diamond, triangle, and square symbols indicate small drifted ice containing IRD, coal, and surface sediment sampling sites in Kongsfjorden and Krossfjorden. See Supplementary Table S1 for detailed sample information on the previously published data. The map was generated using QGIS v3.14 (https://qgis.org/en/site/forusers/visualchangelog314/) based on IBCAOv4 (https://www.ngdc.noaa.gov/mgg/bathymetry/arctic/).

https://doi.org/10.5194/egusphere-2025-957
Preprint. Discussion started: 12 March 2025


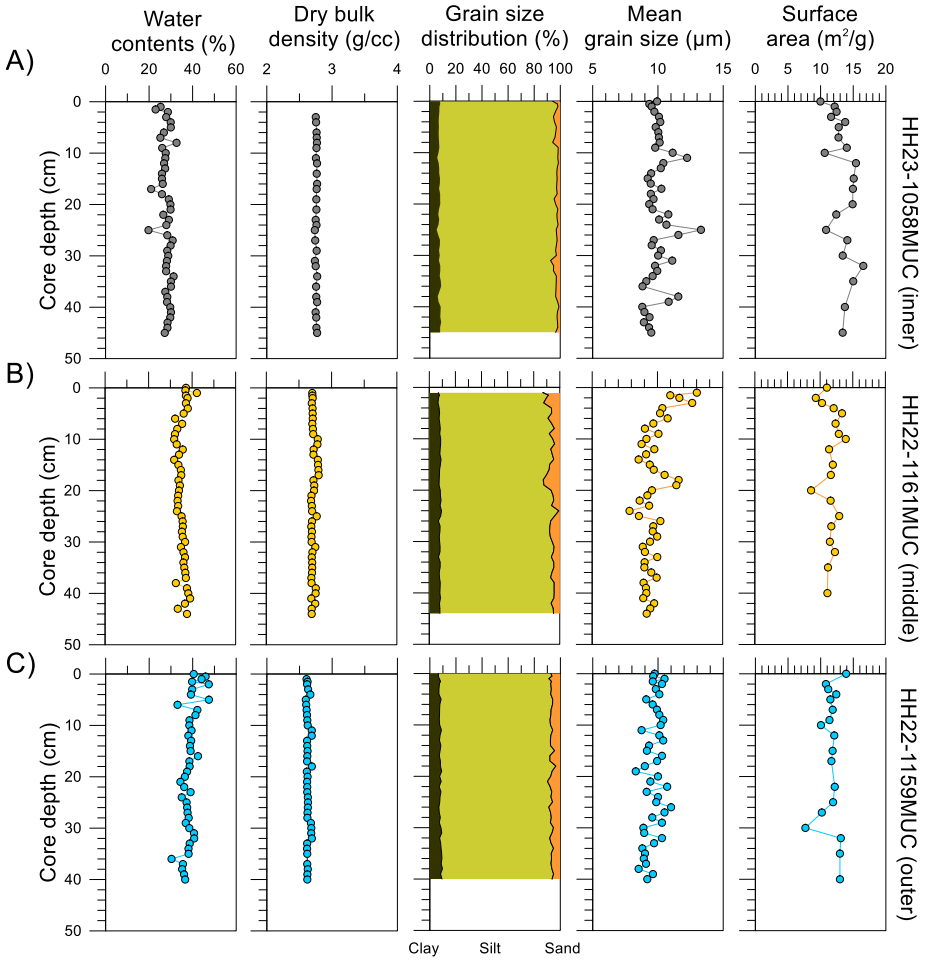


Fig. 2. Depth profiles of water contents (%), dry bulk density (g/cc), grain size distribution (%), mean grain size (μm), and surface area ($m^2/g$) for the cores (A) HH23-1058MUC, (B) HH22-1161MUC, and (C) HH22-1159MUC.

https://doi.org/10.5194/egusphere-2025-957
Preprint. Discussion started: 12 March 2025


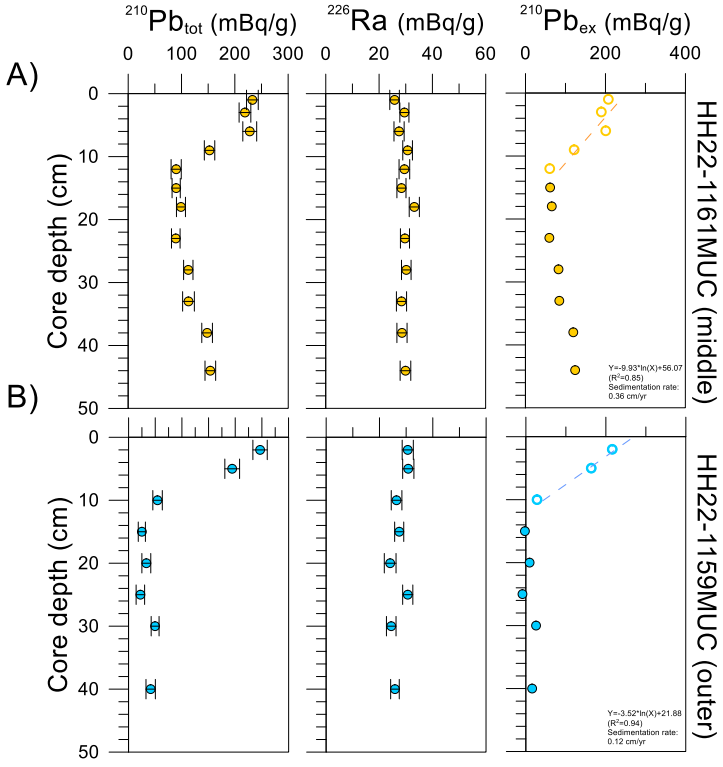


Fig. 3. Depth profiles of $^{210}Pb_{tot}$ (mBq/g), $^{226}Ra$ (mBq/g), and $^{210}Pb_{ex}$ (mBq/g) for the cores (A) HH23-1058MUC, (B) HH22-1161MUC, and (C) HH22-1159MUC.

https://doi.org/10.5194/egusphere-2025-957
Preprint. Discussion started: 12 March 2025


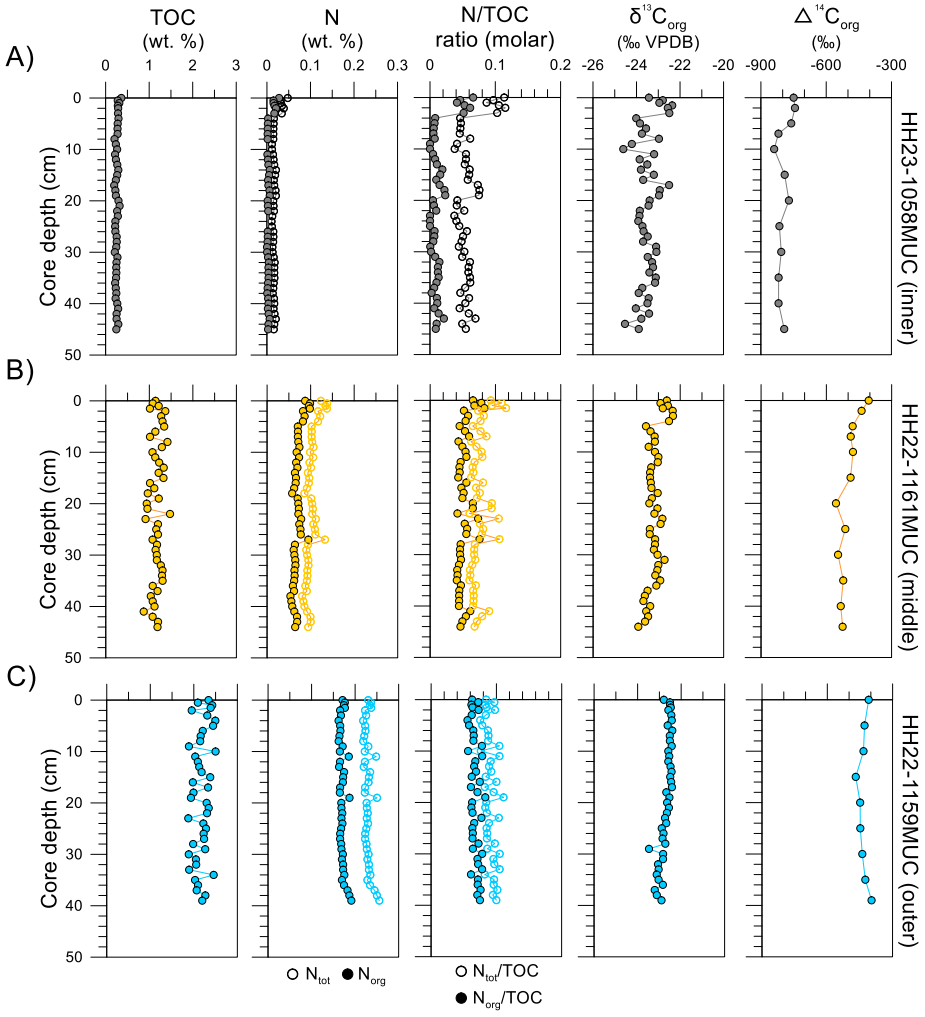


Fig. 4. Depth profiles of TOC (wt. %), N (wt. %), N/TOC ratios (molar), $\delta^{13}C_{org}$ (‰ VPDB), and $\Delta^{14}C_{org}$ (‰) for the cores (A) HH23-1058MUC, (B) HH22-1161MUC, and (C) HH22-1159MUC.

https://doi.org/10.5194/egusphere-2025-957
Preprint. Discussion started: 12 March 2025


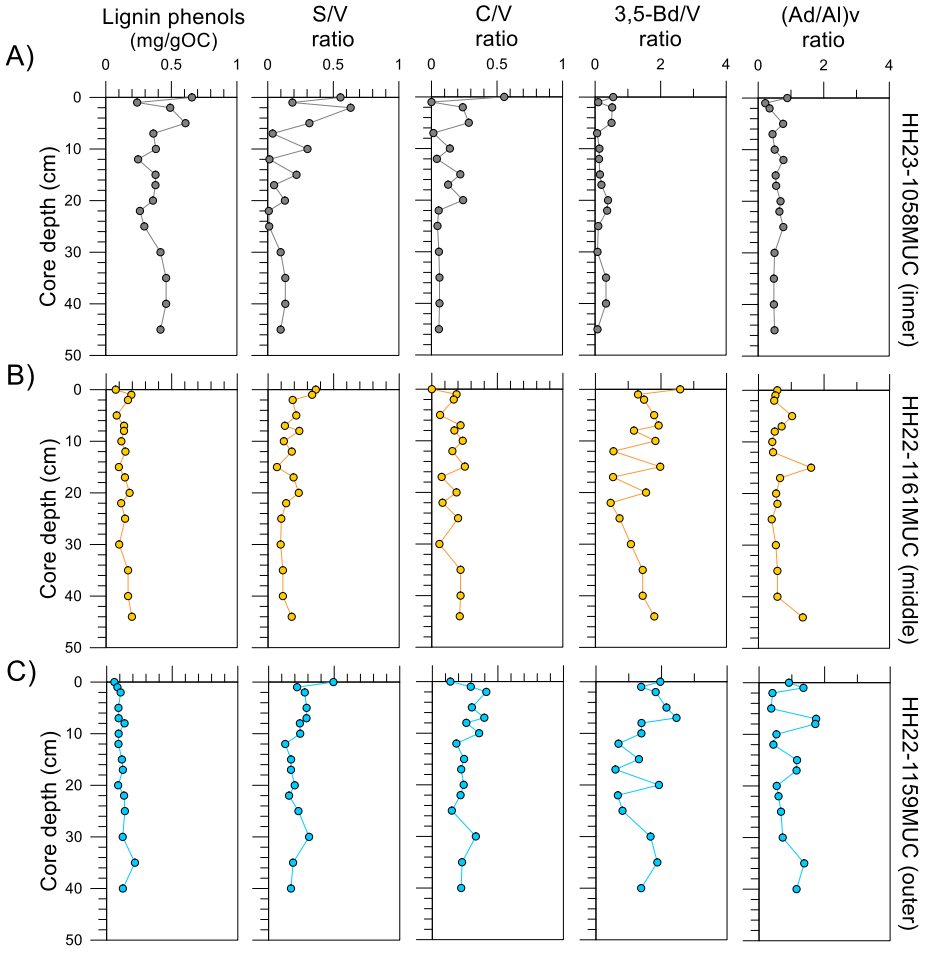


Fig. 5. Depth profiles of lignin phenol concentrations (mg/gOC), and S/V, C/V, 3,5-Bd/V, and (Ad/Al)v ratios for the cores (A) HH23-1058MUC, (B) HH22-1161MUC, and (C) HH22-1159MUC.

https://doi.org/10.5194/egusphere-2025-957
Preprint. Discussion started: 12 March 2025


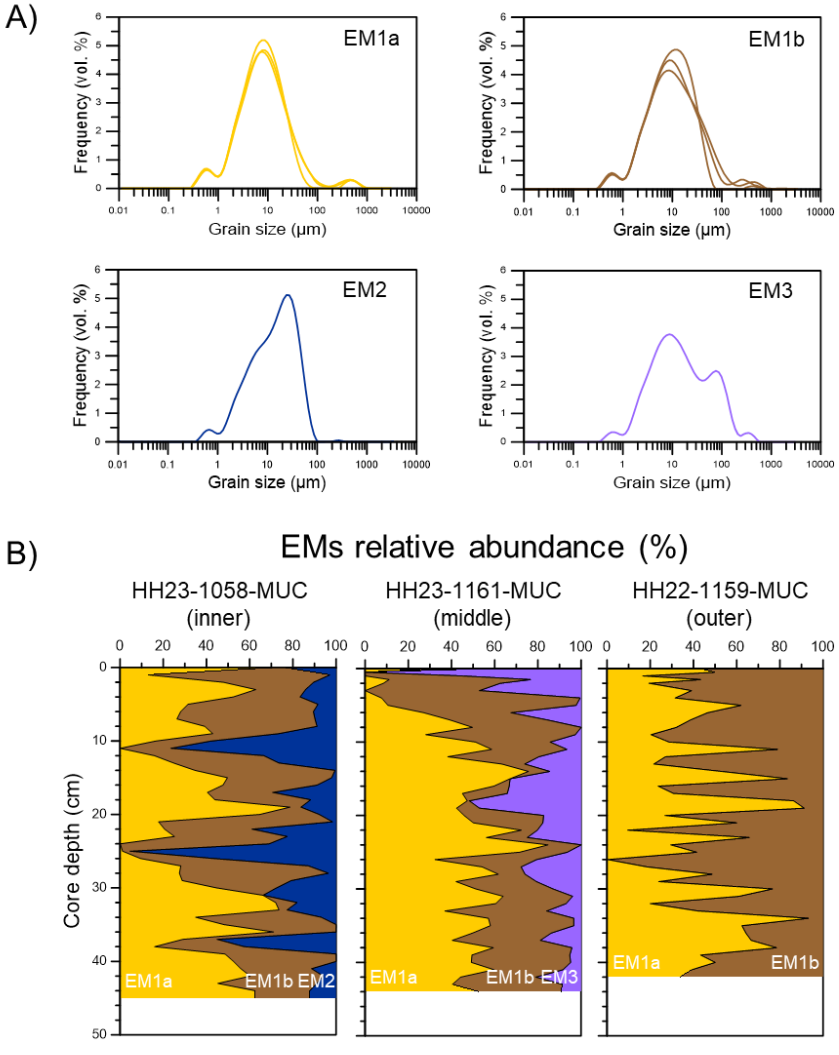


Fig. 6. (A) Classified grain-size end-member distribution curves from three cores, and (B) depth profiles showing the variation in the relative abundances of grain-size end-members (EM1a, EM1b, EM2, and EM3) in the three cores analyzed in this study.

https://doi.org/10.5194/egusphere-2025-957
Preprint. Discussion started: 12 March 2025


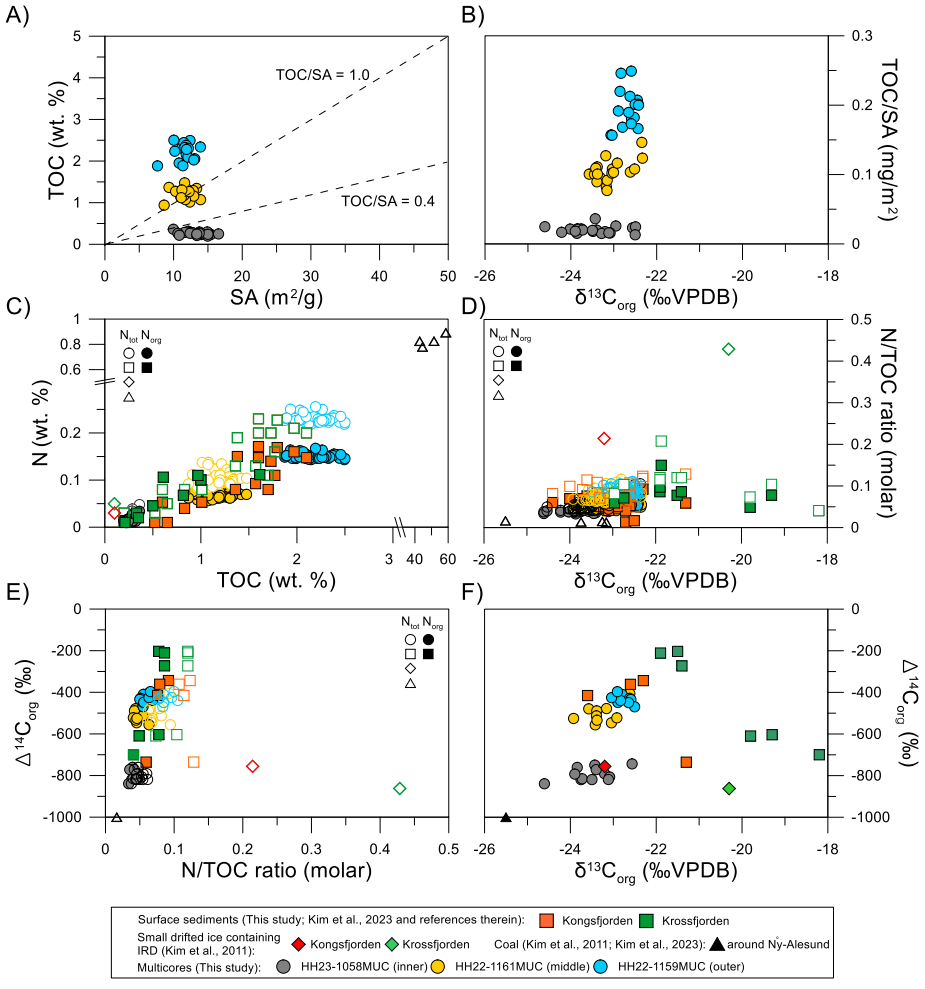


905
906

907 Fig. 7. Scatter plots of (A) SA ($m^2$/g) versus TOC (wt.%), (B) $\delta^{13}C_{org}$ (‰ VPDB) versus
908 TOC/SA (mg/$m^2$), (C) TOC (wt.%) versus $N_{tot}$ or $N_{org}$ (wt.%), (D) $\delta^{13}C_{org}$ (‰ VPDB)
909 versus $N_{tot}$/TOC (molar) ratios or $N_{org}$/TOC (molar) ratios, (E) $N_{tot}$/TOC (molar) ratios or
910 $N_{org}$/TOC (molar) ratios versus $\Delta^{14}C_{org}$ (‰), and (F) $\delta^{13}C_{org}$ (‰ VPDB) versus $\Delta^{14}C_{org}$
911 (‰) for the three cores, compared with data from small drifted ice containing IRD (Kim
912 et al., 2011), coals (Kim et al., 2011; Kim et al., 2023), and surface sediments (Kim et al.,
913 2023 and this study).

https://doi.org/10.5194/egusphere-2025-957
Preprint. Discussion started: 12 March 2025


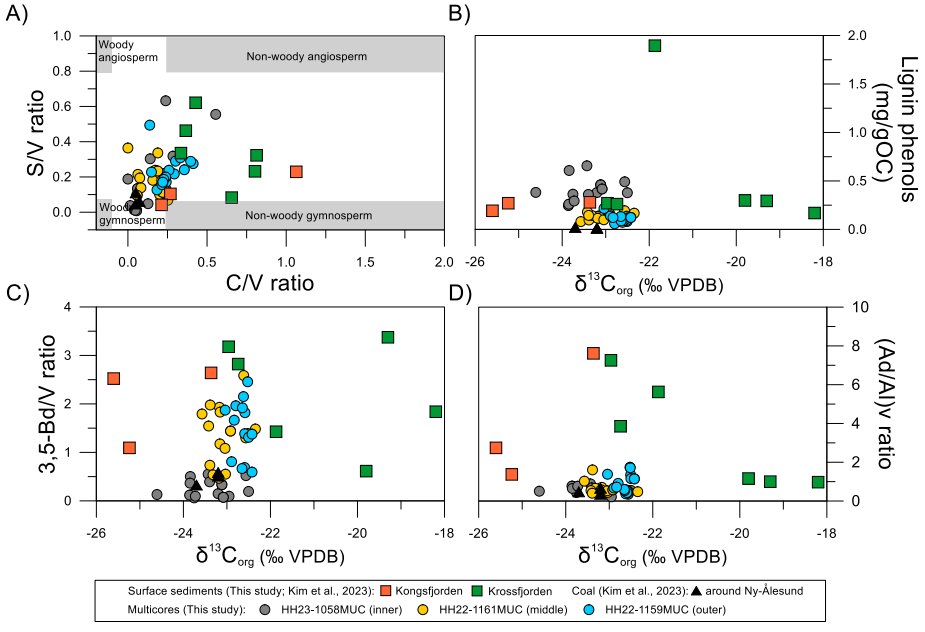


Fig. 8. Scatter plots of (A) C/V ratio versus S/V ratio, including the end-members for different vascular plant tissues (cf. Goñi et al., 2000), (B) $\delta^{13}C_{org}$ (‰ VPDB) versus lignin phenols (mg/gOC), (C) $\delta^{13}C_{org}$ (‰ VPDB) versus 3,5-Bd/V ratio, and (D) $\delta^{13}C_{org}$ (‰ VPDB) versus (Ad/Al)v ratio for the three cores, compared with data from coals (Kim et al., 2023) and surface sediments (Kim et al., 2023 and this study).

https://doi.org/10.5194/egusphere-2025-957
Preprint. Discussion started: 12 March 2025


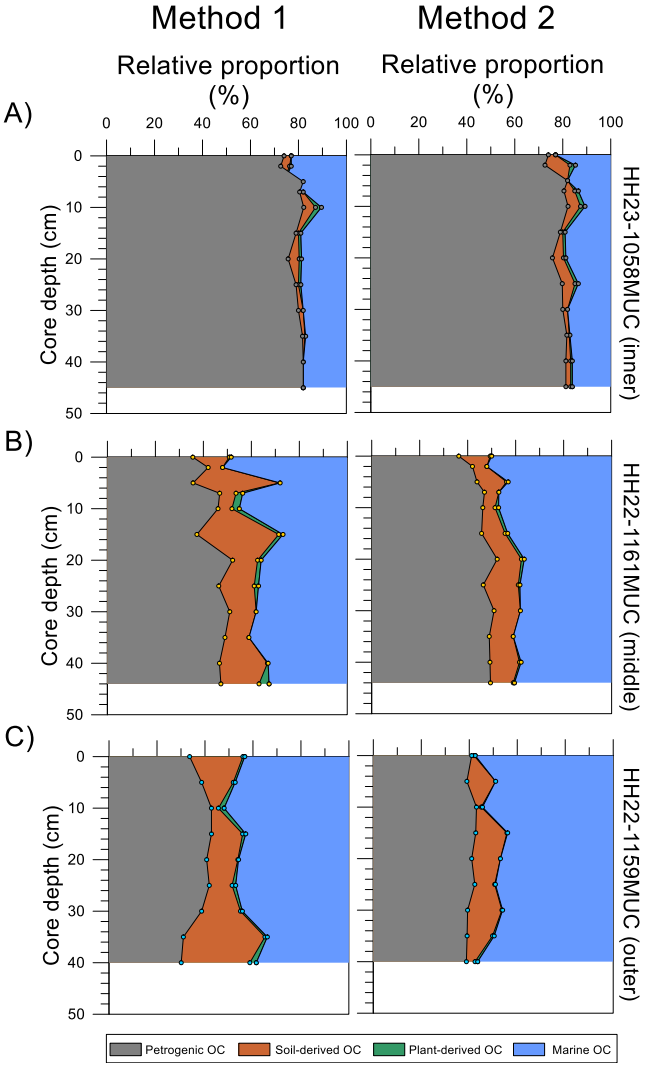


Fig. 9. Depth profiles showing the relative proportions of petrogenic, soil-derived, plant-derived, and marine OC, as determined using Method 1 (based on $\delta^{13}C_{org}$ (‰ VPDB), $\Delta^{14}C_{org}$ (‰), and (Ad/Al)v ratio) and Method 2 (based on $\delta^{13}C_{org}$ (‰ VPDB), $\Delta^{14}C_{org}$ (‰), and lignin phenols (mg/gOC)), for the cores (A) HH23-1058MUC, (B) HH22-1161MUC, and (C) HH22-1159MUC.

https://doi.org/10.5194/egusphere-2025-957
Preprint. Discussion started: 12 March 2025


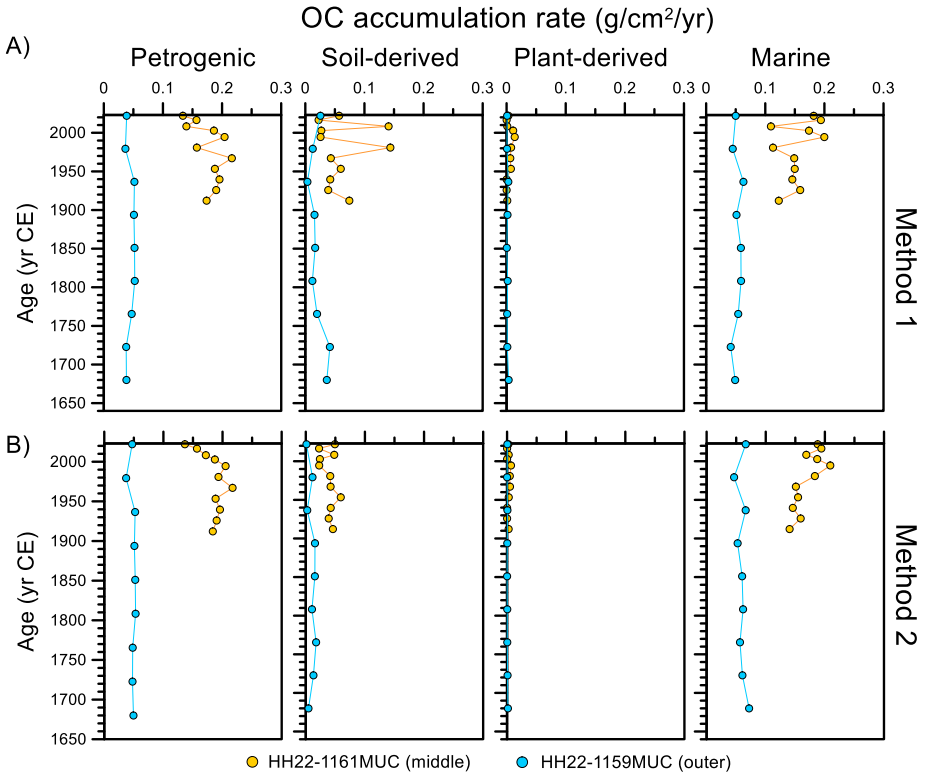


928
929

930 Fig. 10. Age profiles of the accumulation rates (g/cm$^2$/yr) of petrogenic, soil-derived,
931 plant-derived, and marine OC, as determined using Method 1 (based on $\delta^{13}C_{org}$ (‰
932 VPDB), $\Delta^{14}C_{org}$ (‰), and (Ad/Al)v ratio) and Method 2 (based on $\delta^{13}C_{org}$ (‰ VPDB),
933 $\Delta^{14}C_{org}$ (‰), and lignin phenols (mg/gOC)), for the cores HH23-1058MUC, HH22-
934 1161MUC, and HH22-1159MUC.

https://doi.org/10.5194/egusphere-2025-957
Preprint. Discussion started: 12 March 2025


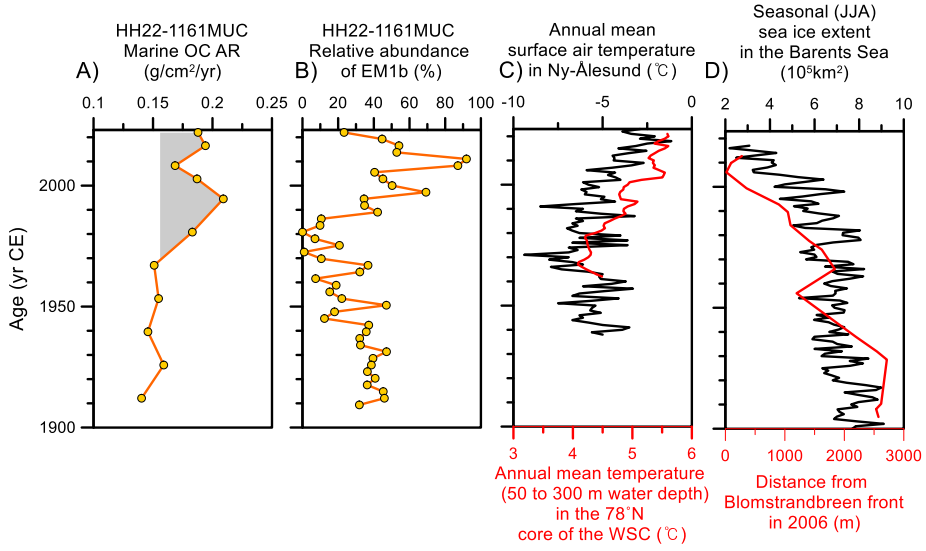


Fig. 11. Age profiles of (A) the accumulation rates of marine OC based on Method 2 for core HH22-1161MUC, (B) the relative abundance (%) of EM1b for core HH22-1161MUC, (C) annual mean surface air temperatures (°C) in Ny-Ålesund (black; data from MOSJ, Environmental monitoring of Svalbard and Jan Mayen) and integrated annual mean temperatures (°C) at 50-300 m water depth in the 78°N core of the West Spitsbergen Current (red; data from MOSJ), and (D) seasonal (JJA) sea ice extent in the Barents Sea (black; data from NSIDC; National Snow and Ice Data Center) and the distance from the Blomstrandbreen front in Kongsfjorden in 2006 (red; data from Burton et al., 2016).